



3D-printed $\lambda/4$ phase plate for broadband microwave applications

YINGWEI WU,¹ PATRICK S. GRANT,¹ AND DMITRY ISAKOV^{2,*}

¹Department of Materials, University of Oxford, Oxford OX1 3PH, UK

²WMG, University of Warwick, Gibbet Hill Road, Coventry CV4 7AL, UK

*d.isakov@warwick.ac.uk

Abstract: An efficient design for a quarter-wave ($\lambda/4$) retardation plate (QWP) operating at microwave frequencies has been designed and manufactured using dual head fused deposition modelling (FDM) 3D printing. Exploiting a bespoke composite material feedstock filament with high dielectric permittivity $\epsilon_r = 10.8$, the resulting 3D-printed QWP comprising alternative layers of high and low permittivity had a high artificial double refraction of $\Delta\epsilon = 2.9$. The QWP provided broadband conversion of linear to circular polarization and phase modulation of an incident plane electromagnetic wave at 12–18 GHz, and demonstrated the potential for optical devices via additive manufacture for use in the microwave frequency range.

Published by The Optical Society under the terms of the [Creative Commons Attribution 4.0 License](https://creativecommons.org/licenses/by/4.0/). Further distribution of this work must maintain attribution to the author(s) and the published article's title, journal citation, and DOI.

The manipulation of the phase distribution of electromagnetic waves may allow encoding of transmitted information and control over the propagation and divergence behaviour of the wave. Consequently, such devices for control of the amplitude, phase and polarization of electromagnetic waves, including phase retarders, beam splitters and polarisers, are of importance in imaging systems and wireless communications [1]. In microwave satellite communication, the phase retarders are the key elements used to mitigate depolarization of the radio link causing the attenuation of the received power due to the troposphere constituents [2]. Polarization converters are also widely used to aid the detection of weak polarised radiation of cosmic microwaves [3].

The intrinsic birefringence of some materials can be used to induce a phase delay between two orthogonal optical axes [4]. However, because natural materials have only limited birefringence, especially for mm-wave and microwave applications, artificial birefringent materials have been developed using non-symmetric and chiral metamaterial resonators [5–9] to achieve more pronounced effects. Achouri *et al.* proposed four birefringent GHz metasurfaces designs to perform operations typical of a $\lambda/2$ plate, a $\lambda/4$ plate, beam splitting and orbital angular momentum multiplexing [10]. A THz narrow-band linear polarization converter with reduced co- and cross-polarised reflections has also been proposed using layered metal grating resonator arrays in a “super-unit-cell” structure placed between polyimide dielectric spacers [11, 12]. Using carefully designed nano-apertures, an ultra-thin plasmonic meta-waveplate exhibited conversion of circular polarised light carrying spin angular momentum into two surface plasmon modes with opposite orbital angular momenta has also been achieved [13].

Alternatively, all-dielectric, non-resonating polarization converters benefit from wide-band, higher transmission and low absorption loss. Prototypes for $\lambda/4$ and $\lambda/2$ plates consisting of a two-dimensional array of elliptical shaped dielectric resonators have been demonstrated in the 20–30 GHz microwave band [14]. Dielectric gradient gratings fabricated by lithography and etching have been shown to possess high transmission, high artificial birefringence, and polarization conversion in the THz regime [15]. An all-dielectric wide-band polarization converter was also fabricated using periodical stacking of rigid foam and polytetrafluoroethylene substrates [16]. Although these examples show there are a variety of demonstrated concepts for phase retarder plates and polarisation converters, the fabrication methods remain bulky, complicated and probably costly. In contrast, the objective of the present work is to design,

simulate and fabricate an all-dielectric polarisation converter with attractive performance that can be readily realised using a simple 3D printing manufacturing approach, with facile extension to many other optical-like devices operating in the microwave regime.

The all-dielectric $\lambda/4$ plate (QWP) design draws on the approach described for a 3D-printed anisotropic dielectric composite possessing Mie-type magnetic resonance in earlier work [17]. This approach comprised 3D-printed mm-scale striped regions of relatively low ϵ_l and high ϵ_h permittivity using Acrylonitrile Butadiene Styrene (ABS) filament and a ABS/BaTiO₃ polymer composite filament respectively [18]. The effective dielectric permittivity ϵ_{eff} of the alternating, high-low permittivity striped structure at microwave frequencies varied with respect to the direction of the electric field E carried by an incident microwave and the volumetric fill fraction v of the high dielectric permittivity material with ϵ_h in the host with relatively low permittivity ϵ_l ($\epsilon_h > \epsilon_l$). The allowed values of the effective permittivity ϵ_{eff} lie in the range between upper (E is parallel to the strips orientation) and lower (E is perpendicular to the strips) Wiener bounds [19]:

$$\epsilon_{\text{max}} = f\epsilon_h + (1 - v)\epsilon_l, \quad (1)$$

$$\epsilon_{\text{min}}^{-1} = v\epsilon_h^{-1} + (1 - v)\epsilon_l^{-1}, \quad (2)$$

Figure 1(a) shows the effective relative dielectric permittivity of the upper (ϵ_{max}) and lower (ϵ_{min}) Wiener bounds of a two-phase composite with $\epsilon_l=2.6$ and $\epsilon_h=10.8$, corresponding to the measured values for ABS and ABS/BaTiO₃ composite filaments [22]. The maximum anisotropy $\Delta\epsilon = \epsilon_h - \epsilon_l$ for a given ϵ_h and ϵ_l will be achieved at an optimum volume fraction v_0 obtained from the solution of the differential equation $\frac{\partial\Delta\epsilon}{\partial v} = 0$:

$$v_0 = \frac{\sqrt{\epsilon_h\epsilon_l} - \epsilon_l}{\epsilon_l - \epsilon_h}, \quad (3)$$

which is also shown graphically in Figure 1(b). For a structure composed of periodic, alternating stripes with $\epsilon_l=2.6$ and $\epsilon_h=10.8$, at a ratio (i.e. filling fraction) $v_0 = 0.67$ the effective dielectric permittivity along the stripes was $\epsilon_{yy}=8.1$ while the permittivity orthogonal to the stripes was $\epsilon_{xx}=5.3$. Thus, due to the difference in phase velocity $c/\sqrt{\epsilon}$, the vertical (E_y) and horizontal (E_x)

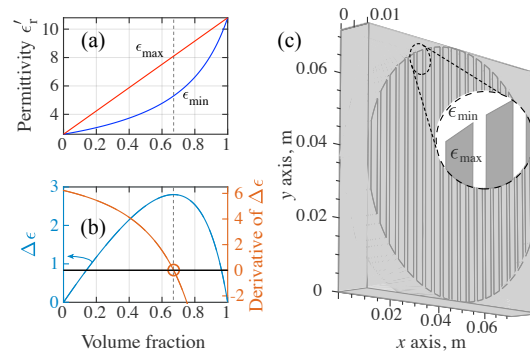


Fig. 1. The design approach for a microwave $\lambda/4$ phase retardation plate. (a) The effective relative dielectric permittivity of the upper (ϵ_{max}) and lower (ϵ_{min}) Wiener bounds as a function of volume fraction v for a two-phase composite with $\epsilon_l=2.65$ and $\epsilon_h=10.8$ corresponding to the experimentally available feedstock filaments for FDM 3D printing. (b) The difference between the upper and lower Wiener bounds $\Delta\epsilon = \epsilon_{\text{max}} - \epsilon_{\text{min}}$ and the corresponding derivative $\Delta\epsilon'(v)$ that determines the optimum volume fraction v_0 , shown as dashed vertical line, at which $\Delta\epsilon = \text{max}$. (c) CAD model of the $\lambda/4$ wave plate composed of two materials and designed with regards to the conditions shown in (b) and from Eq. (6).

components of electromagnetic wave

$$E_y(z, t) = \text{Re}[E_{y0} \exp(j\omega t + kz + \phi_y)] \quad (4)$$

$$E_x(z, t) = \text{Re}[E_{x0} \exp(j\omega t + kz + \phi_x)] \quad (5)$$

(where E_0 is amplitude of the E -field, ω , k and ϕ are angular frequency, wave-vector and phase, respectively) will undergo a time-phase retardation given by:

$$\Delta\phi = \phi_y - \phi_x = \frac{2\pi}{\lambda}(\sqrt{\epsilon_{yy}} - \sqrt{\epsilon_{xx}})d, \quad (6)$$

where d is the thickness of the dielectric anisotropic plate built from the alternating stripes.

Figure 1(c) presents a CAD model of a QWP that implements the periodic alternating structure. Designed for $\lambda = 19.9$ mm (15 GHz), the plate is made of two materials with ϵ_l and ϵ_h with a period of approximately $\lambda/10$ selected to avoid diffraction, and with the relative widths of the stripes determined from Eq. (3). This type of QWP retarder is designed to induce a difference in phase velocity of the orthogonal components of an incident wave so that the relative optical path-length difference between them is $\lambda/4$. It is straightforward to show that implementation of this condition occurs at a relative phase difference $\Delta\phi = \pi/2$. To induce a phase delay of $\pi/2$ between orthogonal components E_y and E_x of the electromagnetic wave incident normally to the plate, the thickness d of the plate can be obtained from Eq. (6) and then all parameters of the 3D model become explicitly defined.

Figure 2 shows simulation results obtained from software COMSOL Multiphysics for a pyramidal horn and a $\lambda/4$ plate inserted in the front of the horn aperture. The pyramidal horn [20] has length 4.4λ and aperture of $3.15\lambda \times 2.45\lambda$ radiating in TM_{01} mode with vertical polarization, and with a theoretical directivity of 18 dBi at 15 GHz. Figures 2(a) and (b) show the near-field orthogonal components of the electric field as a function of propagation distance z for the anisotropic dielectric plate defined as above ($\epsilon_{xx} = \epsilon_{\min} = 5.3$, and $\epsilon_{yy} = \epsilon_{zz} = \epsilon_{\max} = 8.1$) and oriented with its “slow” axis (ϵ_{\max}) along the polarization of the radiated wave, and with the same plate then rotated by 45° , respectively. At 0° orientation in Fig. 2(a), the $\lambda/4$ plate does not change the relative magnitude of the electric field vector, i.e. the polarization. In contrast, rotation of the $\lambda/4$ plate by 45° from this condition (Fig. 2(b)) results in two non-zero components of the

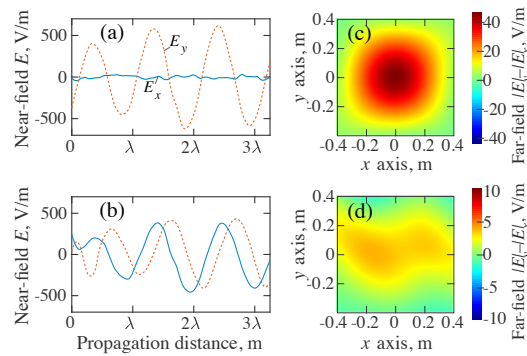


Fig. 2. (a) Simulated near-field x and y components of the electric field E in the direction of radiation for pyramidal horn with E oriented along y -axis and a $\lambda/4$ plate with its “slow” axis also parallel to y . (b) The same components after the rotation of the $\lambda/4$ plate at 45° to the polarization of the horn antenna. (c) Projection of the far-field $|E_y| - |E_x|$ difference on a plane 0.8×0.8 m² at a distance of 100λ from the horn aperture with the $\lambda/4$ plate oriented with its “slow” axis parallel to the radiation polarisation E_y and, (d) oriented at 45° . Note that the intensity contours in the colour legend have different scales.

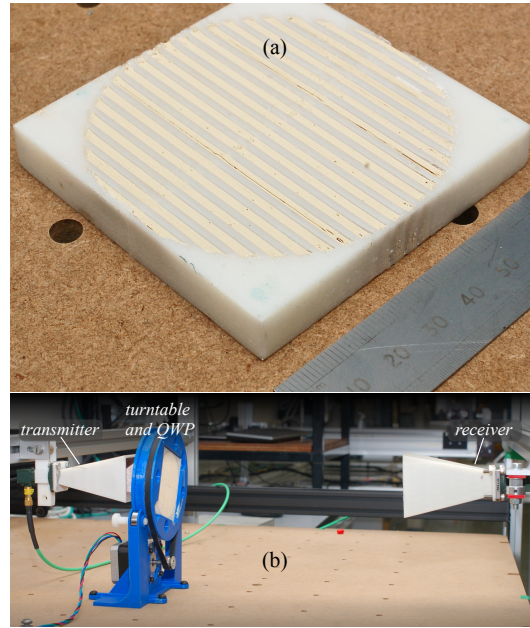


Fig. 3. (a) Photograph of the 3D-printed $\lambda/4$ plate and (b) experimental setup.

E -field polarization with equal amplitude and a $\pi/2$ relative phase shift, corresponding to circular polarization. Figures 2(c) and 2(d) show a 2D map of the amplitude difference $|E_y^{\text{far}}| - |E_x^{\text{far}}|$ at a distance of 100λ from the horn (far-field), again for 0 and 45° orientations of the $\lambda/4$ plate, respectively. On rotation of the plate, $|E_y^{\text{far}}| - |E_x^{\text{far}}|$ reduces to ≈ 0 .

Following the above design and simulated proof-of-concept, a QWP was fabricated by two-head FDM 3D printing as described previously [21] using bespoke ABS/BaTiO₃ composite high-permittivity filament [22] and commercial ABS filament (Fig. 3(a)). The complex dielectric permittivity of both materials was characterised at 15 GHz by the split-post resonator method [23] as $\epsilon_h = 10.8 - j0.038$ and $\epsilon_l = 2.6 - j0.008$ for composite and ABS filaments respectively. The performance of the 3D-printed QWP was assessed experimentally using the arrangement shown in Fig. 3(b) and schematically in Fig. 4(a). The QWP was placed between two rectangular flange pyramidal horns facing each other at approximately 25λ distance, referred hereafter as a polariser (P, transmitted horn) and analyser (A, receiver horn), by analogy with visual optics. The two orthogonal components E_y and E_x of the transmitted signal (power gain) were analysed separately, at relative orientation of the A horn to the P horn of either 0° or 90° along the transmission direction and with the interposed QWP plate fixed at 45° , i.e. P0-QWP45-A0 and P0-QWP45-A90 conditions, respectively. Figure 4(b) shows the difference of the power gains between these two conditions while Fig. 4(c) shows the phase difference $\Delta\phi = \phi_y - \phi_x$ obtained at the two orientations.

As described above, a circularly polarised wave must follow two conditions: $|E_x| = |E_y|$ and a phase difference $\pm(\frac{1}{2} + 2n)\pi$ ($n = 0, 1, 2, \dots$). Although the QWP was designed for 15 GHz, the experimental data from Figs. 4(b) and (c) show that these conditions were best realised at 13.1 GHz, 14.4 GHz, 15.7 GHz, and 16.35 GHz. The negative sign of $\Delta\phi$ in Fig. 4(c) was indicative of left-handed circular polarisation. The non-zero power gain difference in Fig. 4(b) suggested slight elliptical character of the E -field polarization in the 12–18 GHz frequency range, rather than perfectly circular.

Figure 4(d) presents the transmitted wave amplitude as a function of rotation angle θ of the

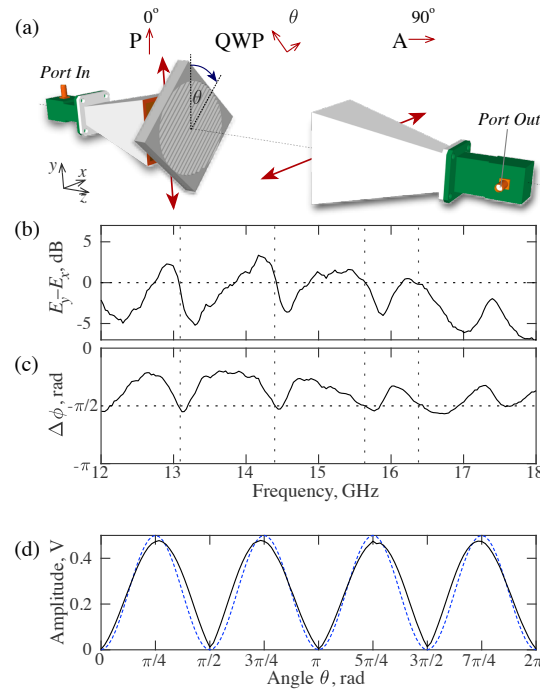


Fig. 4. (a) Schematic of the experimental setup showing two pyramidal horns and the $\lambda/4$ plate. (b) Measured power gain difference and phase difference (c) between transmitted E_y ($P \parallel A$) and E_x ($P \perp A$) components with $\lambda/4$ plate oriented at 45° to the principal axes. (d) Measured transmittance (solid black curve) as a function of the $\lambda/4$ plate rotation between two ports oriented perpendicularly to each other ($P \perp A$).

QWP inserted between P and A horns fixed at 90° relative rotation (Fig. 4(a)), measured at 15.7 GHz. The transmission function T of such an optical system can be assessed theoretically using Jones calculus [24] as:

$$T = \frac{1}{2} \sin^2(2\theta). \quad (7)$$

A plot of Eq. (7) is also shown in Fig. 4(d) as a dashed curve, with very good fit to the experiment. The small deviations were attributed to non-ideal alignment of the QWP with respect to the propagation direction, possible printing defects, and radiation losses.

In summary, our results reveal the potential for using inexpensive FDM 3D printing for the manufacture of electromagnetic optical-like devices operating in the GHz frequency range. These RF devices are scaled-up from optical device dimensions and then readily fabricated by additive manufacture in a single operation. A 3D-printed QWP operated efficiently close to 15 GHz using a simple design comprising parallel strips of polymer and composite materials with alternating high-low dielectric permittivity with an artificial effective dielectric anisotropy $\Delta\epsilon = 2.9$. At an optimum fraction of high permittivity stripes and orientation to incident radiation, a linearly polarised microwave underwent conversion to E -field circular polarisation with close to the theoretical character. The proposed design of the QWP makes it possible to use this device in a beamforming line with flat optics. Employing a QWP arrangement in conjunction with a computer-controlled rotation table with automatic adjustment of orientation could be used to readily maximize the magnitude of the transmission signal in a communication line.

Funding

UK Engineering and Physical Sciences Research Council, grant EP/P005578/1.

References

1. N. J. G. Fonseca and C. Mangenot, "High-Performance Electrically Thin Dual-Band Polarizing Reflective Surface for Broadband Satellite Applications," *IEEE Trans. Antennas Propag.* **64**, 640 (2016).
2. A. Ghasemi, A. Abedi, and F. Ghasemi, *Propagation Engineering in Wireless Communications*, 2nd Ed., Springer International Publishing, Switzerland, 2012.
3. S. A. Bryan, T. E. Montroy, and J. E. Ruhl, "Modeling dielectric half-wave plates for cosmic microwave background polarimetry using a Mueller matrix formalism," *Appl. Optics* **49**, 6313 (2010).
4. M. Born and E. Wolf, *Principles of Optics: Electromagnetic Theory of Propagation, Interference and Diffraction of Light*, 6th Ed., Cambridge Univ. Press, UK, 1993.
5. J. Hao, Y. Yuan, L. Ran, T. Jiang, J. A. Kong, C. T. Chan, and L. Zhou, "Manipulating electromagnetic wave polarizations by anisotropic metamaterials," *Phys. Rev. Lett.* **99**, 063908 (2007).
6. Z. Wei, Y. Cao, Y. Fan, X. Yu, and H. Li, "Broadband polarization transformation via enhanced asymmetric transmission through arrays of twisted complementary split-ring resonators," *Appl. Phys. Lett.* **99**, 221907 (2011).
7. J. Y. Chin, J. N. Gollub, J. J. Mock, R. Liu, C. Harrison, D. R. Smith, and T. J. Cui, "An efficient broadband metamaterial wave retarder," *Opt. Express* **17**, 7640 (2009).
8. X. Huang, D. Yang, and H. Yang, "Multiple-band reflective polarization converter using U-shaped metamaterial," *J. Appl. Phys.* **115**, 103505 (2014).
9. H. Shi, A. Zhang, S. Zheng, J. Li, and Y. Jiang, "Dual-band polarization angle independent 90° polarization rotator using twisted electric-field-coupled resonators," *Appl. Phys. Lett.* **104**, 034102 (2014).
10. K. Achouri, G. Lavigne, and C. Caloz, "Comparison of two synthesis methods for birefringent metasurfaces," *J. Appl. Phys.* **120**, 235305 (2016).
11. N. K. Grady, J. E. Heyes, D. R. Chowdhury, and Y. Zeng, "Terahertz metamaterials for linear polarization conversion and anomalous refraction," *Science* **340**, 1304 (2013).
12. W. Mo, X. Wei, K. Wang, Y. Li, and J. Liu, "Ultrathin flexible terahertz polarization converter based on metasurfaces," *Optics Express* **24**, 13621 (2016).
13. H. Yang, G. Li, X. Su, G. Cao, Z. Zhao, F. Yu, X. Chen, and W. Lu, "Annihilating optical angular momentum and realizing a meta-waveplate with anomalous functionalities," *Opt. Express* **25**, 16907 (2017).
14. A. Yahyaoui, H. Rmili, K. Achouri, M. Sheikh, A. Dobaie, A. Affandi, and T. Aguilu, "Transmission Control of Electromagnetic Waves by Using Quarter-Wave Plate and Half-Wave Plate All-Dielectric Metasurfaces Based on Elliptic Dielectric Resonators," *Int. J. Antenna Prop.* **2017**, 8215291, (2017).
15. M. Chen, F. Fan, S.-T. Xu, and S.-J. Chang, "Artificial high birefringence in all-dielectric gradient grating for broadband terahertz waves," *Sci. Rep.* **6**, 38562 (2016).
16. M. Lorente-Crespo, G. C. Ballesteros, G. Goussetis, and C. Mateo-Segura, "Experimental Validation of All-Dielectric mm-Wave Polarization Conversion Based on Form Birefringence," *IEEE Microw. Wireless Compon. Lett.* **26**, 759 (2016).
17. D. Isakov, Q. Lei, F. Castles, C.J. Stevens, C.R.M. Grovenor, and P. S. Grant, "3D printed anisotropic dielectric composite with meta-material features," *Mat. Des.* **93**, 423 (2016).
18. F. Castles, D. Isakov, A. Lui, Q. Lei, C. E. J. Dancer, Y. Wang, J. M. Janurudin, S. C. Speller, C. R. M. Grovenor, and P. S. Grant, "Microwave dielectric characterisation of 3D-printed BaTiO₃/ABS polymer composites," *Sci. Rep.* **6**, 22714 (2016).
19. D. E. Aspnes, "Bounds on allowed values of the effective dielectric function of two-component composites at finite frequencies," *Phys. Rev. B Condens. Matter* **25**, 1358 (1982).
20. C. A. Balanis, *Antenna Theory: Analysis and Design*, John Wiley & Sons, Inc. USA, 1997.
21. D. Isakov, C.J. Stevens, F. Castles, and P. S. Grant, "3D-Printed High Dielectric Contrast Gradient Index Flat Lens for a Directive Antenna with Reduced Dimensions," *Adv. Mater. Technol.* **1**, 1600072 (2016).
22. Y. Wu, D. Isakov, and P. Grant, "Fabrication of Composite Filaments with High Dielectric Permittivity for Fused Deposition 3D Printing," *Materials* **10**, 1218 (2017).
23. J. Krupka, "Developments in techniques to measure dielectric properties of low-loss materials at frequencies of 1–50 GHz," *J. Europ. Ceram. Soc.* **23**, 2607 (2003).
24. A. Yariv, *Optical Electronics*, 4th Ed. (Saunders College Publishing, USA, 1991).